Communication in Physical Sciences 2020, 5(4): 575-591

Chemical synthesis and characterization of zinc, iron and carbon-based nanoparticles and their nanocomposites

Comfort M. Ngwu, Steven A. Odoemelam* and Jude C. Nnaji
Received 20 June 2020/Accepted 17 July 2020/Published online: 25 August 2020

Abstract *The wet chemical approach (an aspect of the bottom-up method) was used to synthesize zinc oxide, magnetite and graphene oxide, graphene oxide/magnetite and chitosan/magnetite nanoparticles and their nanocomposites. The synthesized particles were characterized by FESEM/EDX, FT-IR and XRD techniques. Zinc oxide was obtained with a crystallite size of 9.0 nm. The synthesized magnetite particles had a crystallite particle size of 6.4 nm. Crystallite sizes obtained for GO, GO-magnetite and chitosan-magnetite were 7.9, 7.1 and 11.2 nm, respectively. The synthesized composite did not display any phase change in the magnetite.*

Key Words: *Nanoparticles, nanocomposites, grapheme oxide, zinc oxide, magnetite, chitosan*

Comfort M. Ngwu
Department of Chemistry, Michael Okpara University of Agriculture, Umudike, P.M.B 7267 Umuahia, Abia State, Nigeria
Email: kom4tngwu@gmail.com
Orcid id: 0000-0003-4723-2813

Stevens A. Odoemelam*
Department of Chemistry, Michael Okpara University of Agriculture, Umudike, P.M.B 7267 Umuahia, Abia State, Nigeria,
Email: saodoemelam@gmail.com
Orcid id:

Jude C. Nnaji
Department of Chemistry, Michael Okpara University of Agriculture, Umudike, P.M.B 7267 Umuahia, Abia State, Nigeria
Email: judennaji30@gmail.com
Orcid id: 0000- 0002-5569-4818

1.0 Introduction

Research in nanotechnology has recorded a huge progress in recent times due to the utilization of nano materials in diverse fields including mechanics, optics, biomedical sciences, chemical industry, electronics, space industries, drug delivery, energy science, catalysis, photoelectrochemical applications, agriculture, environmental remediation (Iravani, 2011; Odiongenyi and Afangide, 2019; Odiongeny, 2019). One of the unique properties of nano materials is that they can be presented in different forms such as, nanowires, nanotubes, films, particles, quantum dots, composites and colloids (Edelstein and Cammaratra, 1998; Lubick and Betts, 2008). Their novel nanoscale size confers on them certain interesting properties and abilities such as large surface area, quantum effect, electrochemical and magnetic properties, and other size-dependent physical and chemical properties (Keiner, 2008) The design of nanomaterials with novel applications can be achieved by controlling its shape and size at the nanoscale. This can be achieved through physical, chemical or biological processes operating through bottom-up or top-down approach, which entails the progressive cutting of a mass material to get the nanosized material. Modification of nanomaterials by coupling them to bioactive components is another synthesis method. The integration of nanoparticles with biodegradable materials results in new nanomaterial having distinct properties such as size, surface chemistry, roughness (Ramos *et al.,* 2017).

Development of cost effective and scalable synthetic methods for nanomaterials has attracted serious challenges and has led to numerous researches in the field have of nano science. The bottom-up approach is widely preferred synthetic route for nanomaterials because of the high-cost, energy intensive, complex and technical set up of the top down approach. Also, the nanomaterials produced in the top down procedure seldom have wide applicability because of their surface defects and non-uniformity in shape. To a good extent, the bottom-up approach is much associated with the wet chemical

synthesis method, which employs chemical reductants, chemical precipitation, sol-gel synthesis, and solvothermal/hydrothermal reaction, photochemical reduction and laser irradiation technique (Liu *et al*. 2015; Kumar *et al.,* 2017, Wang and Xia, 2004). The wet chemical synthesis approach has been observed to effectively produce and replicate nanomaterials of desirable size and shape, in addition, the process is facile, modular and innovative (Pottathara *et al.,* 2019).

Various nanomaterials have been synthesized using the wet chemical process. For example, Fe_3O_4 nanoplates with an average edge length of 80 nm through microwave irradiation was synthesized by Zhou *et al.,* (2010). Savasari *et al.*, used ascorbic acid to produce stabilised zero valent iron nanoparticles assembled in a chain in which individual particles were round in shape with a diameter of 20 to 75 nm. Magnetic chitosan nanoparticles were also synthesized by Chang *et al*. (2006), having an average diameter of 13.5 nm as a magnetic nano-adsorbent. This was done by the carboxy methylation of chitosan, followed by immobilization on the Fe_3O_4 nanoparticles surface through carbodiimide activation. Ren *et al.* (2013) reported the synthesis of a novel magnetic EDTA-modified chitosan/SiO2/Fe3O4 adsorbent through surface modification of chitosan/SiO2/Fe3O4 (CMS) with EDTA using water-soluble carbodiimide as the cross-linker in buffer solution. The synthesized nanomaterials were characterized using Raman scattering (SERS). Transmission electron microscopy (TEM), Fourier infrared spectrometry (FT-IR), X-ray diffraction (XRD), and vibrating sample magnetometer (VSM) (Ren *et al.,* 2013). According to Dhillon *et al.* (2014), ZnO–chitosan nanoparticles were synthesized by the nano spray drying and precipitation methods, using citric acid, glycerol, starch and whey powder as stabilizers. Both synthetic methods were simple, eliminating the use of toxic chemicals. The characterization of the nanoparticles was carried out using UV–Vis spectroscopy, dynamic light scattering particle size analysis, zeta potential measurements and scanning electron microscopy, which confirmed the synthesis of NPs with varying shapes and sizes.

In this study, a bottom up approach using the wet chemical procedure is adopted for the synthesis of five different inorganic nanoparticles and composites, i.e., zinc oxide (ZnO), magnetite (Fe_3O_4), graphene oxide (GO), magnetite/graphene oxides (Fe_3O_4-GO) and magnetite/chitosan, which have potential applications in environmental remediation, medical and pharmaceutical fields.

2.0 Materials and Methods

2.1 Reagents

Analytical grade zinc acetate dihydrate, $Zn(CH_3COO)_22H_2O$, sodium carbonate Na_2CO_3, ethanol (C_2H_5OH) (Sigma-Aldrich), Chitosan was provided by Prof. Lee of the Department of Chemistry, University of Saskatoon, Canada. Iron (III) chloride hexahydrate ($FeCl_3.6H_2O$), acetic acid, sodium hydroxide, and 25 % ammonia solution, Graphite powder (99.95%) (Sigma-Aldrich), sodium nitrate ($NaNO_3$), potassium permanganate ($KMnO_4$), hydrogen peroxide (H_2O_2), hydrogen chloride (HCl) and ammonium chloride (NH_4Cl). All other reagents were purchased from BDH Chemicals Limited, Poole, England. Reagents were used as received without further purification and deionized water was used to prepare all solutions.

2.2.1 Synthesis of zinc oxide nanoparticles

ZnO NP was prepared by the precipitation method as described by Fouad *et al.,* (2011) and Mohamed *et al.,* (2012), with slight modification. 14.8 g (0.148 moL) of $Zn(CH_3COO)_2.2H_2O$ and 13.8 g (0.138 moL) of Na_2CO_3 were mixed at room temperature. The mixture was vigorously stirred until a white precipitate was obtained. The precipitate formed was filtered and washed thoroughly with distilled water and absolute ethanol, and dried at 100 °C for 6 h. The $Zn(CH_3COO)_2.2H_2O$ was converted to ZnO nanoparticles, while the Na_2CO_3 was converted to CH_3COONa. The equation of the reaction is as shown below:

$$Zn(CH)_3(COO)_{2\ (s)} + Na_2CO_{3\ (s)} \rightarrow ZnO\ (s) + CH_3COONa(aq) + CO_{2(g)} \quad (1)$$

2.2.2 Synthesis of magnetite nanoparticles (M.NPs)

Magnetite nanoparticles were also prepared via chemical precipitation as described by Khalil (2015). Aqueous solution (A) was prepared by dissolving 27.30 g of $FeCl_3.6H_2O$ (27.03 g) in 150 mL distilled water. 5.533 g (0.033 mol) of potassium iodide was also dissolved in 50.0 mL of distilled water to prepare aqueous solution B. Solutions A

and B were mixed together at room temperature, stirred and allowed to attain equilibrium for 1 h. The precipitate of iodine was filtered out, and washed with distilled water. The washing was added to the filtrate and the entire volume of filtrate was hydrolyzed using 25 % ammonia solution which was added drop-wise with constant stirring to enhance complete precipitation of the black magnetite at a pH of 10. The system was left to settle after which it filtered, washed with distilled water and dried at a temperature of 250 °C.

2.2.3 Synthesis of graphene oxide (GO)

Graphene oxide powder was prepared according to the modified Hummer's method. Graphite powder (10 g), 10 g $NaNO_3$, 450 ml of concentrated H_2SO_4 were added to 1000 ml volumetric flask in ice bath and stirred continuously for 4 hours. 60 g of $KMnO_4$ was slowly added (below 15 ºC), for 30 minutes. The mixture was diluted with 900 ml of deionized water and stirred for 2 hours continuously at 35 ºC. The system was further refluxed at 98 ºC (10-15 minutes) until brown colour was obtained. The mixture was treated with 200 ml H_2O_2 till the solution became bright yellow while stirring continued for an hour in the presence of doubly distilled water. The mixture was finally centrifuged with 10 % HCl and deionized water. Gel-like substance formed was vacuum dried at 60 ºC for 6 hours.

2.2.4 Synthesis of GO-Fe_3O_4 nanocomposite

Synthesis was done according to the method proposed by Genc-Fuhrman *et al.,* (2004). GO-Fe_3O_4 nanocomposite was prepared by adding 20 g of GO, (dry weight) in 250 ml solution of 50 mg of $FeCl_3$ and 25 g of $FeCl_2$ respectively. The solution was heated at 85 ºC, and 30 % ammonia solution was added to adjust the pH to 10. After stirling for 45 minutes, the solution was allowed to cool to room temperature, filtered, and rinsed with deionized water to obtain the GO-Fe_3O_4 suspension. To obtain the GO-Fe_3O_4 particles, the suspension was dried at 70 ºC, followed by grinding and sieving to a 40-mesh particle size.

2.2.5 Synthesis of chitosan/magnetite nanocomposite

The procedure described by Unsoy *et al.,* (2012) was used in the synthesis of chitosan-magnetite nanoparticles with slight modifications: Chitosan (5 g), was dissolved in 2 % aqueous acetic acid solution. The previously prepared fine magnetite nanoparticles (2.5 g) was dispersed in 50 ml ethanol and sonicated for 20 minutes, and then added drop-wisely to the chitosan solution under high-speed mechanical stirring for homogenization. The composite obtained was precipitated in a mixture of 5 % NaOH and ethanol and was filtered. After filtration, the composite was washed several times and vacuum dried to constant weight.

2.2.6 X-ray diffraction (XRD)

The crystalline forms of the nanoparticles were quantified by measuring their X-ray diffraction patterns, using a high-resolution Bruker D8 Advance diffractometer of Cu Kα (λ = 1.54050 Å) radiation. The samples (1 g) were scanned from 15° to 90° 2 theta range with a step size of 0.02 ° and a step rate of 0.454° s^{-1}. The crystallite size was calculated from XRD pattern with the help of the Debye-Scherrer equation given as, $D = K\lambda / \beta\cos\theta$ where D is crystallite size (nm), λ is the wavelength of X-rays (1.54050 Å), β exhibits the full width of the peak at half maximum (FWHM) and cos θ is Bragg angle (rad). K is Scherrer constant (0.94) related to crystallite shape.

2.2.7 FTIR Analysis

Infrared spectra were obtained by using a Fourier transform infrared spectrophotometer (FTIR) (Perkin-Elmer Spectrum RX1). The analysis was performed to confirm the presence of surface functional groups. The powder samples (99 mg) were properly mixed with 1 mg of potassium bromide (KBr) and pressed into pellets under vacuum, until they appeared clear and not translucent. The pellets were then carefully removed from the disc, placed in the FTIR sample holder and analyzed by the transmission mode with a resolution of 4 cm^{-1}. The spectra of the different samples were recorded in the wavenumber range of 4000 to 400 cm^{-1}.

2.2.8 FE-SEM/EDX Analysis

The surface morphology of synthesized nanoparticles at different magnifications was studied using Field emission scanning electron microscopy equipped with an energy dispersive X-ray (EDX) detector (FESEM) (ZEISS ultra plus). To be observed with a SEM, 20 mg of the samples were first made conductive for current. This was done by coating them with an extremely thin layer (1.5 - 3.0 nm) of gold-palladium for sputtering.

3.0 Results and Discussion

3.1 FESEM Analysis

3.1.1 FESEM with EDX images of ZnO nanoparticles

Fig. 1 a &b show the SEM images of the ZnO nanoparticles at different magnifications while Fig. 2 shows the elemental mapping. From the results obtained, it is evident that the ZnO nanoparticles had flake-like, and porous morphology with less aggregation. Sangeetha *et al.* (2011) and Rosi and Merkin, (2005) have reported similar observations. The size observed for ZnO sample by FESEM was within the range, 9-50 nm range. EDX of the samples shown in Fig. 2(a-c) displayed peaks of C, Zn and O atoms and confirms the presence of ZnO nanoparticles. The percentage error corresponding to Zn and O are in good agreement with permissible error. The presence of C, Zn and O are in accordance with equation of the synthesis. EDX mapping images of ZnO are presented in Fig. 2(f) where the Zn and O elements are clearly detected, confirming the formation of ZnO structure.

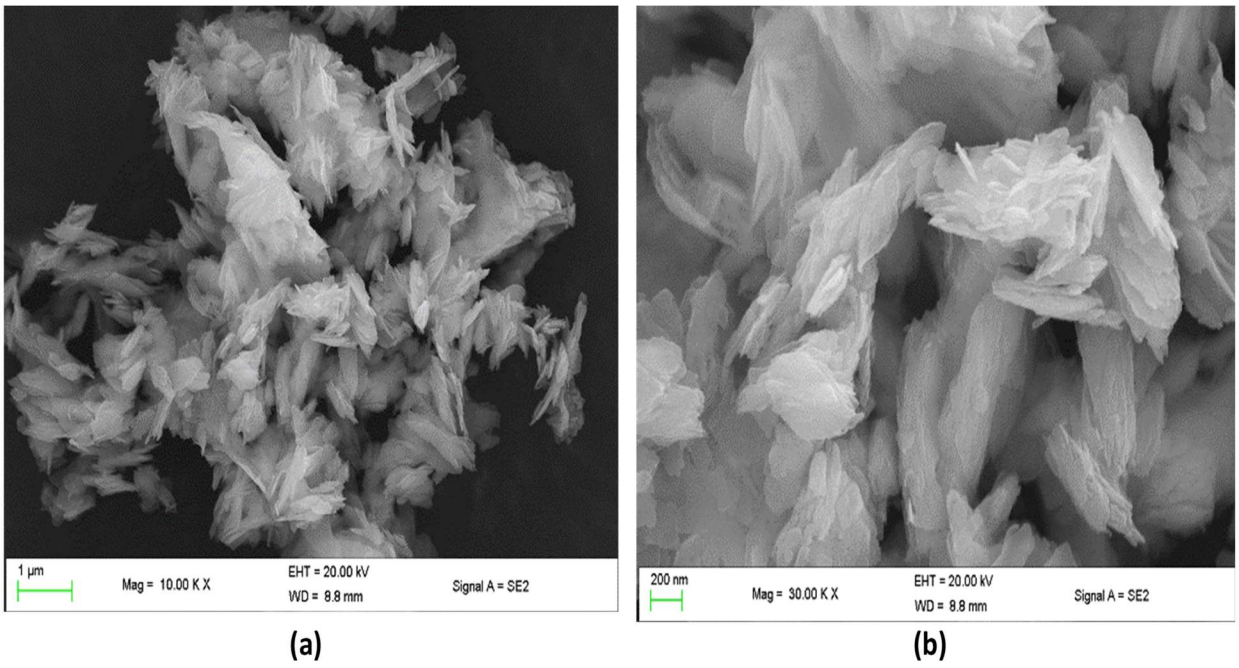

Fig. 1 (a-b): SEM images of ZnO nanoparticles at different magnifications

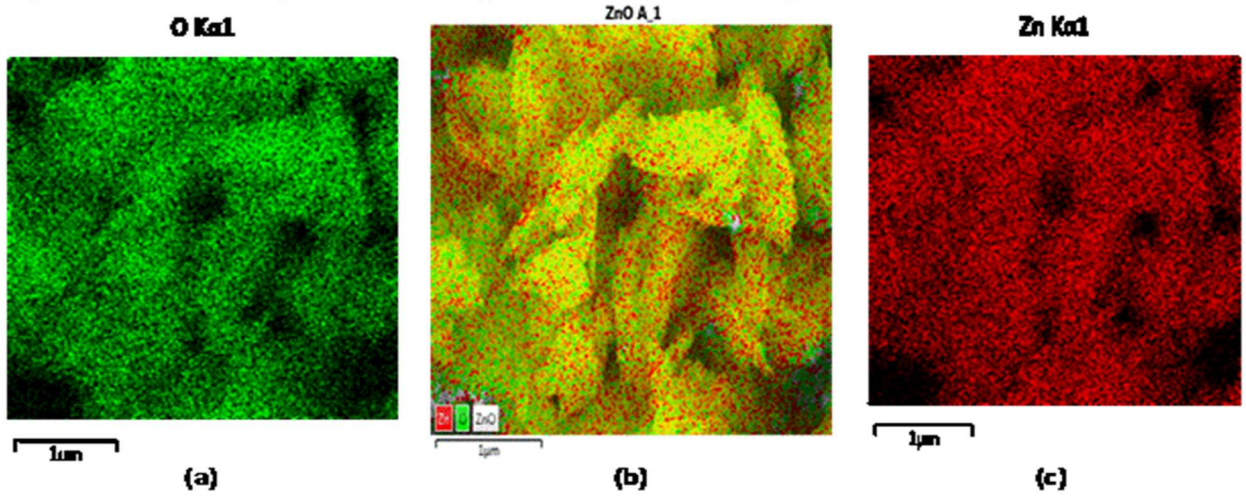

Fig. 2 (a-c): Elemental mappings of ZnO.

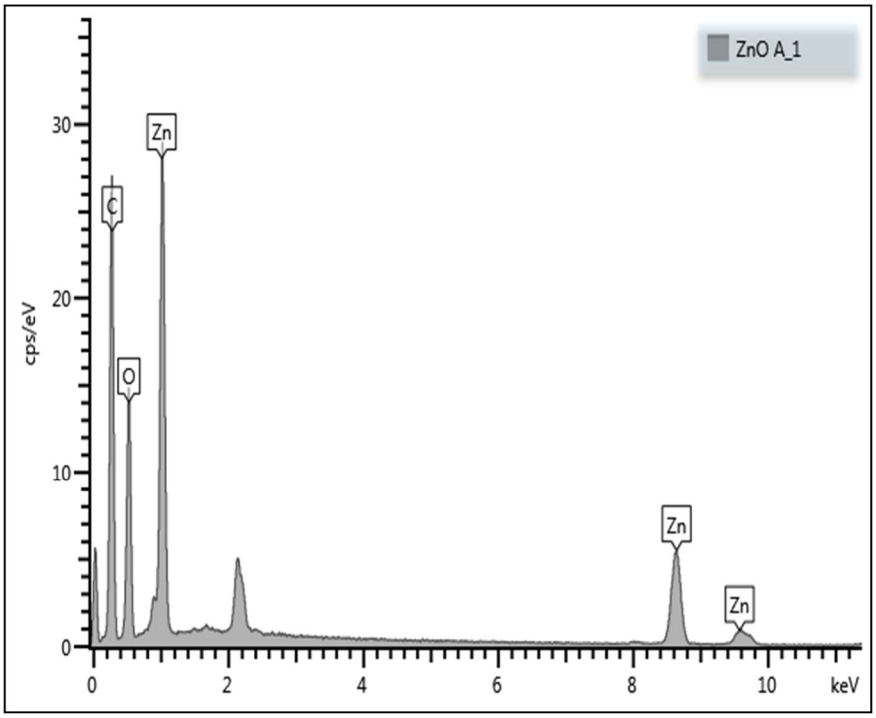

ZnO A_1	Wt%	Wt% Sigma
C	56.96	0.27
O	25.59	0.24
Zn	17.44	0.17
Total	100.00	

Fig. 2f: EDX spectra of synthesized ZnO nanoparticles

3.1.2 FESEM with EDX images of magnetite nanoparticles

The SEM images of magnetite shown in Fig. 3 (a&b), reveals the presence of aggregates with different shapes and lengths, formed by agglomerated and almost spherical nanoparticles. The agglomeration is due to magnetic dipole interactions between the particles (Eldin, *et al.,* 2012). The estimated size of nanoparticles (5-17 nm) after examination by SEM analysis is in good agreement with the values of calculated crystallite size obtained from XRD analysis. The presence of Fe and O in the EDX spectra and elemental mappings in Fig 3 (c-f) confirmed the formation of magnetite nanoparticles.

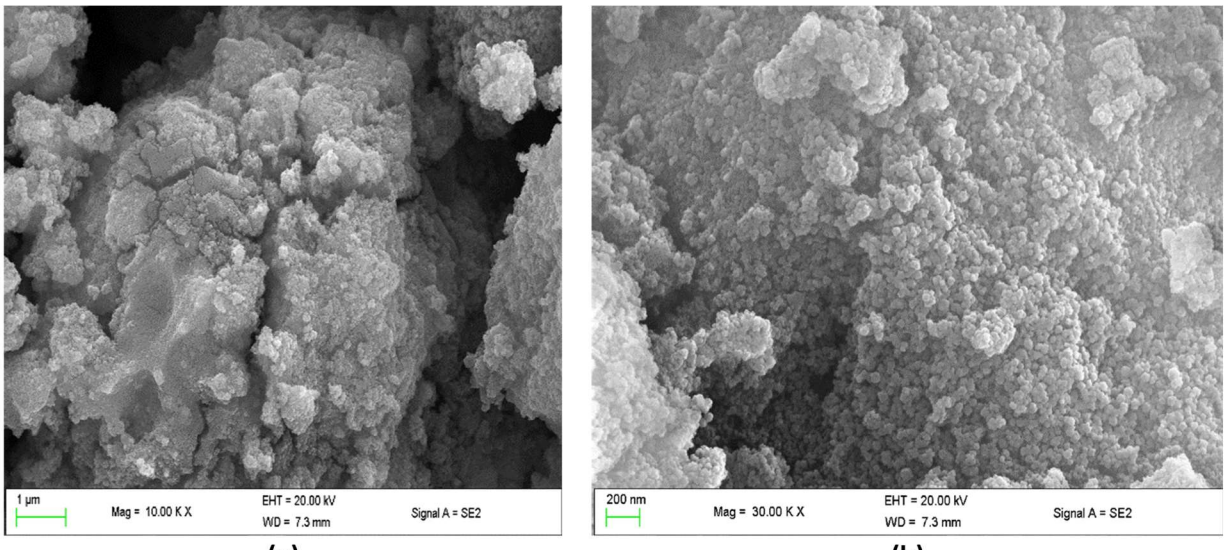

(a) (b)

Fig. 3 (a - b): FESEM images of synthesized nano magnetite at different magnifications

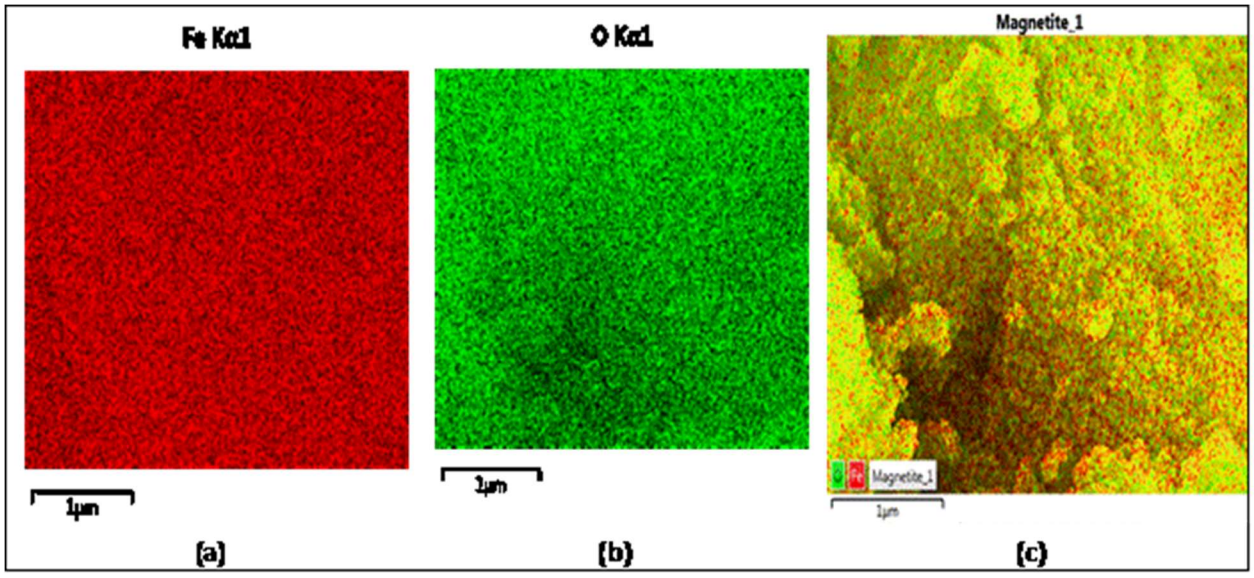

Fig. 3(c-e) :Elemental mapping of nanomagnetite

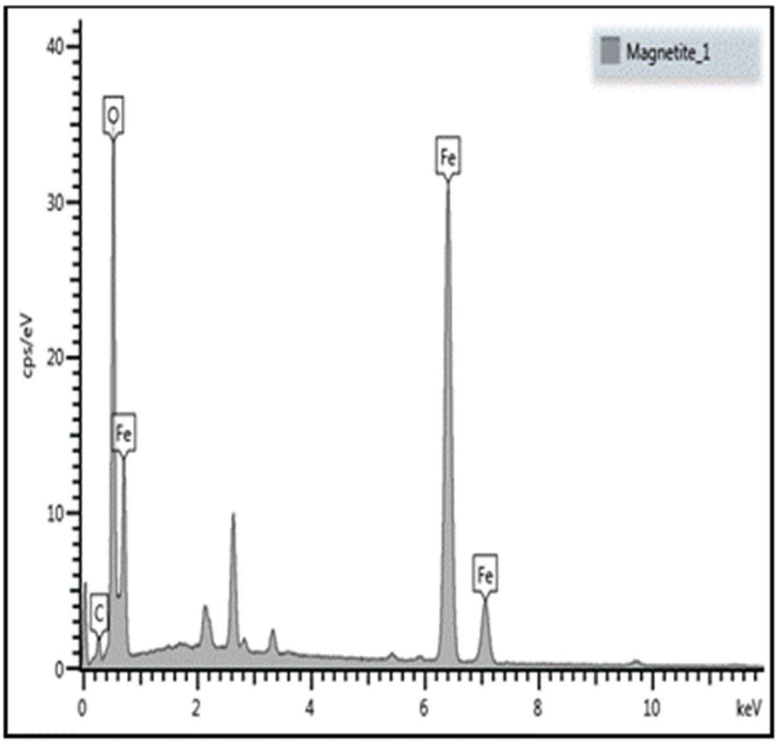

Magnetite_1	Wt%	Wt% Sigma
C	7.68	0.35
O	33.82	0.22
Fe	58.51	0.28
Total	100.00	

Fig. 3 :EDX spectra of synthesized magnetite nanoparticles

3.1.3 FESEM with EDX images of Graphene oxide

Surface morphology of the synthesized graphene oxide was also observed with FESEM. images of the graphene oxide (GO) nanoparticles (Fig 4 a and b) and they reveal well defined and interlinked three-dimensional graphene oxide sheets, forming a porous network that resembles a loose sponge-like structure. A number of GO sheets are seen layered onto each other, which resulted in the agglomeration of GO, this multilayered structure, confirms the formation of GO (Ayrat and James, 2014). Elemental composition and mappings determined by EDX is shown in Figs 4 (c-f), the weight percentage of carbon and oxygen were obtained as 65.47 % and 34.35 % respectively. A negligible amount of iron was also observed as impurity.

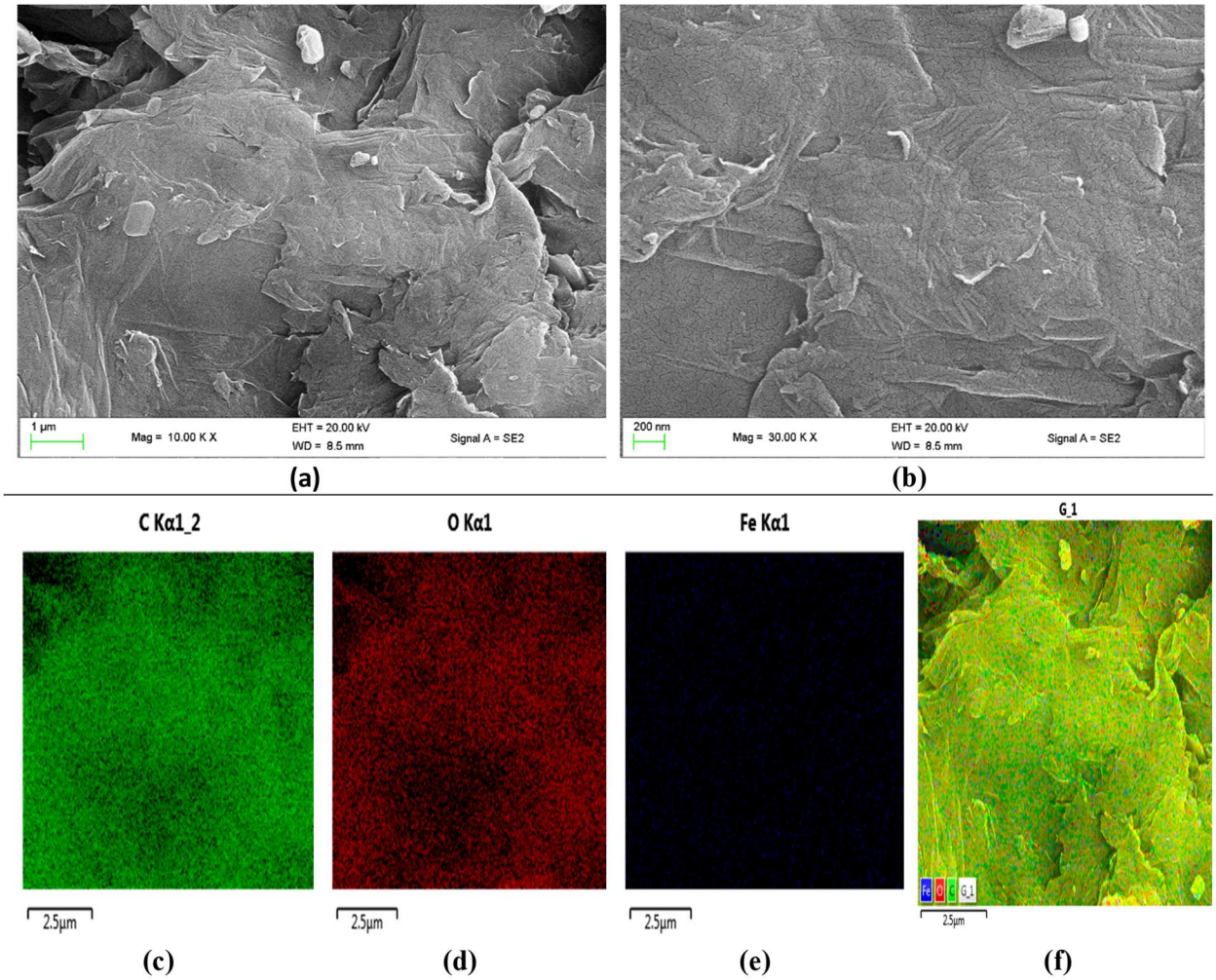

Fig. 4: FESEM images of synthesized GO nanocomposite (a-b) and elemental mapping of GO nanocomposite (c-f)

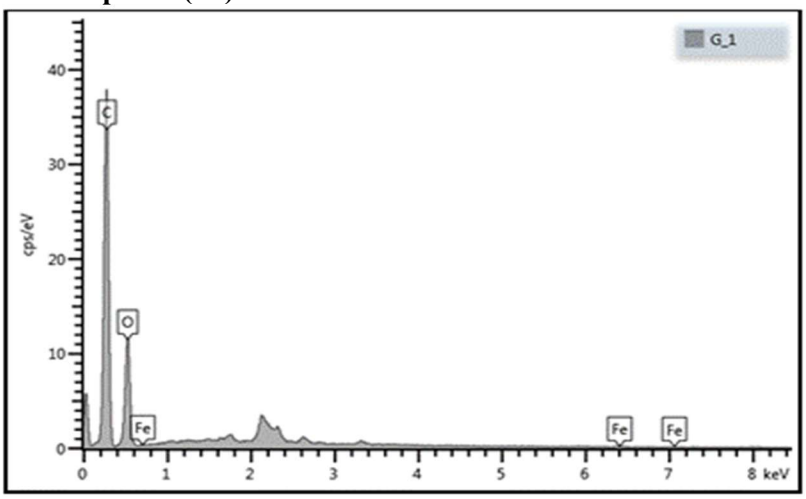

G_1	Wt%	Wt% Sigma
C	65.47	0.37
O	34.35	0.37
Fe	0.18	0.05
Total	100.00	

Fig. 4g :EDX spectra of Synthesized GO nanocomposite

3.1.4 FESEM with EDX images of Graphene oxide-magnetite nanoparticles

The morphology of synthesized graphene oxide-magnetite nanocomposite obtained from FESEM is as shown in Fig. 5 (a & b). The graphene oxide sheets were disorderly distributed between the closely packed Fe_3O_4 nanoparticles. Nano-sized Fe_3O_4 anchored on GO uniformly, resulting in well combination between GO and Fe_3O_4. Bright spheres were also observed all over the surface of the graphene sheets indicating successful formation of Fe_3O_4 nanoparticles on the surface of graphene oxide (Zubir *et al.,* 2014). The average particle size of GO-magnetite composite was estimated to be 6.4 nm. Fig. 5 (c-f) also shows the elemental mappings of the nanocomposite. Further investigation using EDX analysis (Fig.5 (g)) confirmed the elemental composition of the GO-Magnetite nanocomposite, in which the elements C, O and Fe were present in various compositions as indicated.

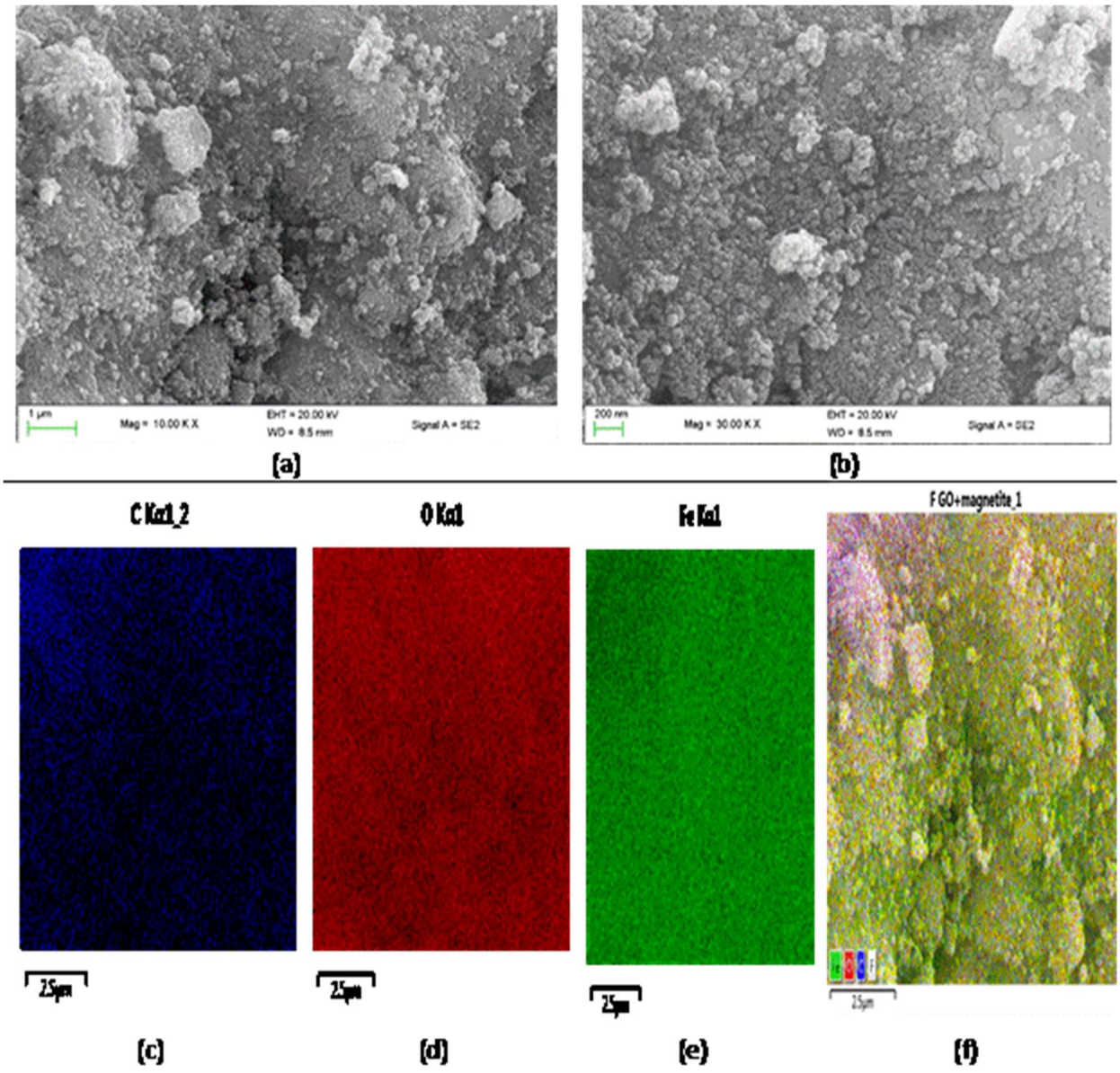

Fig.5: FESEM images of synthesized GO-magnetite nanocomposite (a-b) and elemental mappings of GO-Magnetite nanocomposite (c-e)

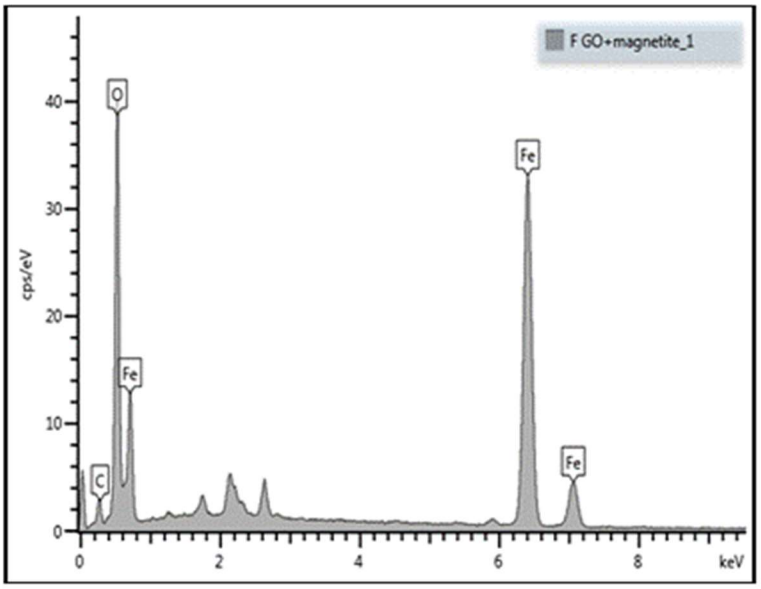

F GO+magnetite_1	Wt%	Wt% Sigma
C	10.05	0.41
O	35.38	0.26
Fe	54.57	0.32
Total	100.00	

Fig. 5(g): EDX spectra of Synthesized GO-magnetite nanocomposite

3.1.5 FESEM with EDX images of chitosan-magnetite nanoparticles

The FESEM images of chitosan-magnetite nanocomposite (Fig 6(a-b) showed partly agglomerated tiny spherical beads that are evenly distributed.

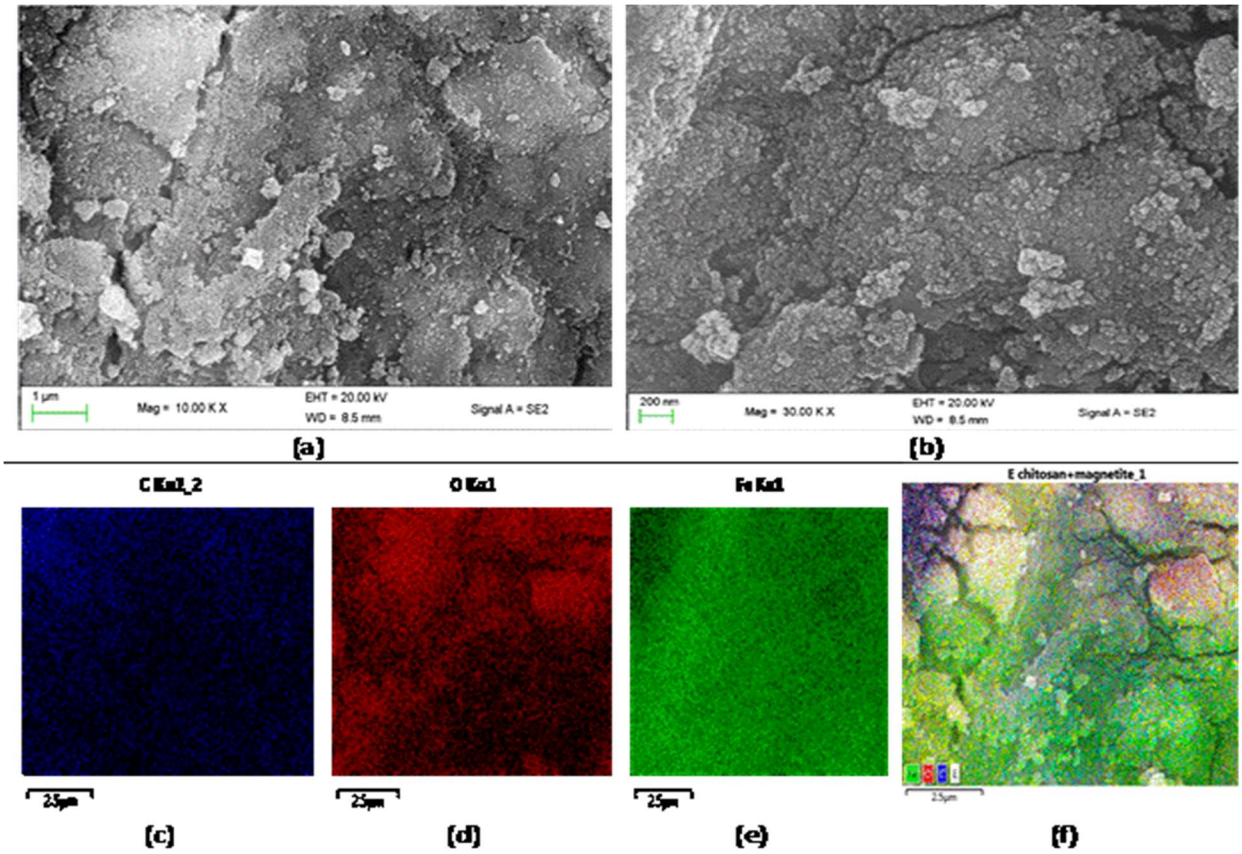

Fig. 6 :FESEM images of synthesized chitosan-magnetite nanocomposite(a-b) and elemental mappings of chitosan-magnetite nanocomposite (c-f)

The electron dispersive spectroscopy (EDX) analysis of these particles indicated the presence of Fe and O composition in the chitosan–magnetite nanocomposite (Fig. 6f). The elemental composition of iron, oxygen and carbon were 44.76, 23.78 and 31.46 %, respectively. The results obtained are in agreement with the work of Vaishnavi *et al.* (2015) who reported the composition of iron and oxygen in iron oxide nanoparticles to be 52.71 and 34.88 %, respectively. No other peak related to any impurity was detected in the EDX, which confirms that the grown nanoparticles in the nanocomposite were composed only of iron, oxygen and carbon. Thus, the presence of iron content in the nanocomposite was confirmed from the EDX results.

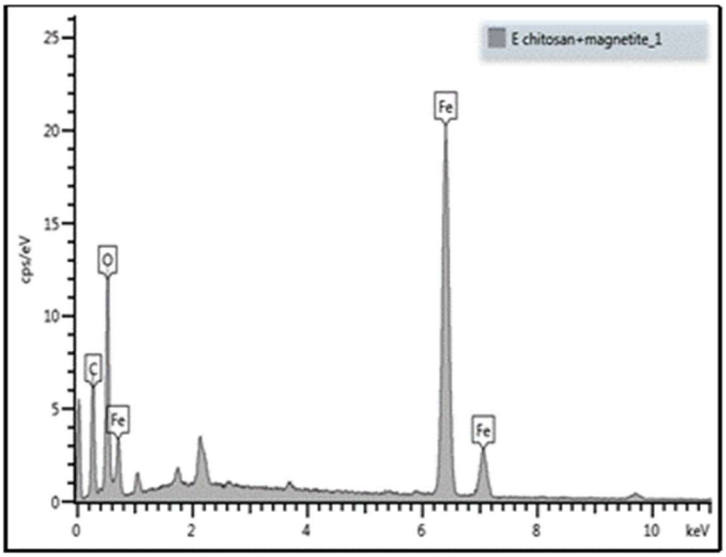

E chitosan+magnetite_1	Wt%	Wt% Sigma
C	31.46	0.46
O	23.78	0.31
Fe	44.76	0.36
Total	100.00	

Fig. 6f EDX spectra of synthesized chitosan-magnetite nanocomposite

3.2 Fourier-Transform Infrared Spectroscopy (FTIR)

3.2.1 FTIR spectra of ZnO nanoparticles

Fig. 7 shows the FTIR spectrum of ZnO nanoparticles. The peak at 468 cm^{-1} is typical for the absorption of Zn-O bond. The band at 676 cm^{-1} indicates the stretching vibrations of ZnO nanoparticle. The intense peaks at 1384 and 1500 cm^{-1} are attributed to symmetrical and asymmetrical stretching of the zinc carboxylate groups while the observed absorption at 831 cm^{-1} is due to the lattice vibration of CO_3^{-2} (Wang *et al.,* 2010). This also verifies that Na_2CO_3 was one of the precursors used in the synthesis of ZnO nanoparticles. The weak double peaks at 2159 and 2026 cm^{-1} are typical for C-H aldehydic stretching vibration. Broadband observed around 3500 cm^{-1} is assigned to O–H stretching mode of the hydroxyl group. This result is in good agreement with those reported by others (Zaka *et al.,* 2011, Hong *et al.,* 2009).

3.2.2 FTIR spectra of Fe_3O_4 nanoparticles

In the FTIR analysis of magnetite (Fig. 8) the presence of absorption bands at 449, 538 and 2352 cm^{-1} correspond to the magnetite (Fe_3O_4) phase. The bands observed at 684 cm^{-1} corresponded to the intrinsic stretching vibration (Fetetra ↔ O) of metal-oxygen at tetrahedral site whereas the band at 449 cm^{-1} corresponds to the stretching vibration (Feocta ↔ O) of metal-oxygen at octahedral site. Another related report showed that the characteristic absorption bands of the Fe-/O bond of bulk Fe_3O_4 were in 570 and 375 cm^{-1} (Ma *et al.,* 2003). However, in the synthesized magnetite, these two bands shifted to high wavenumbers of about 538 and 449 cm^{-1} respectively. The peaks at 1609 and 3120 cm^{-1} may be attributed to the stretching vibration of the –OH group of adsorbed water on the surface of the magnetite nanoparticles.

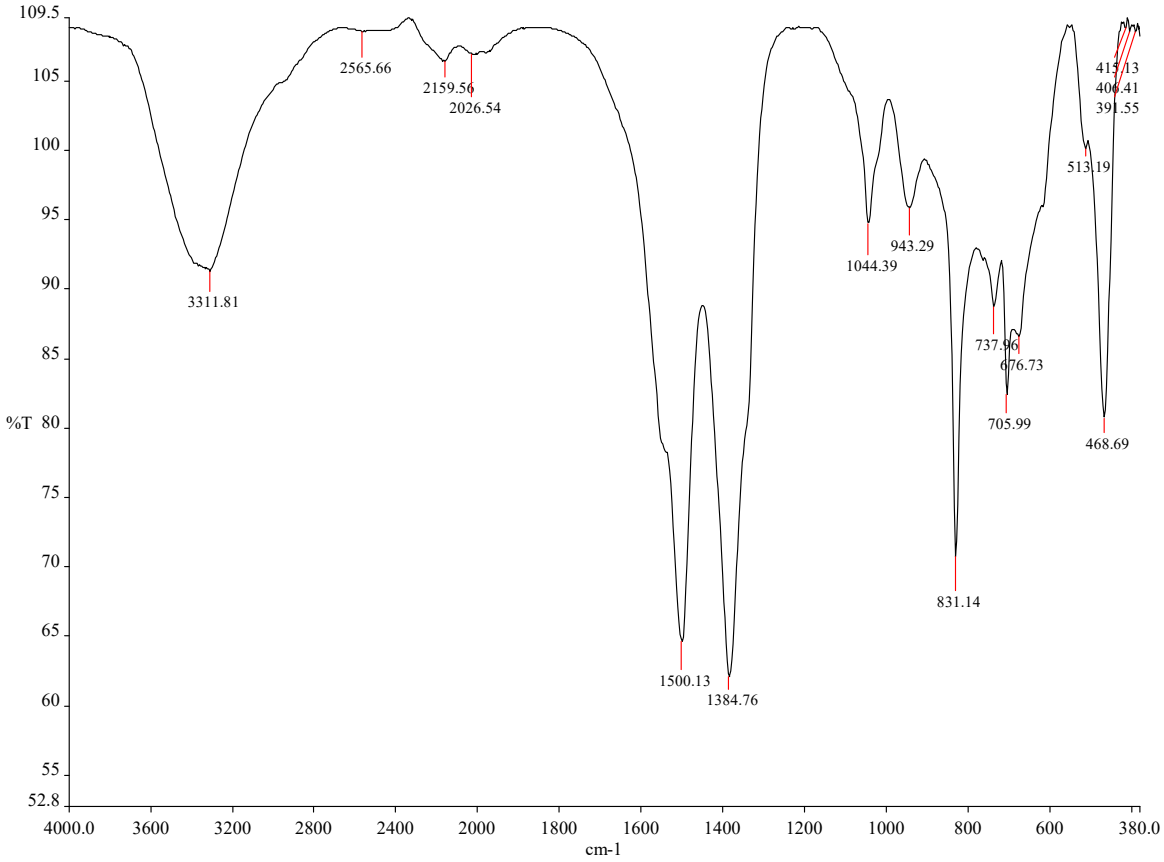

Fig. 7 FTIR spectrum of synthesized ZnO nanoparticles

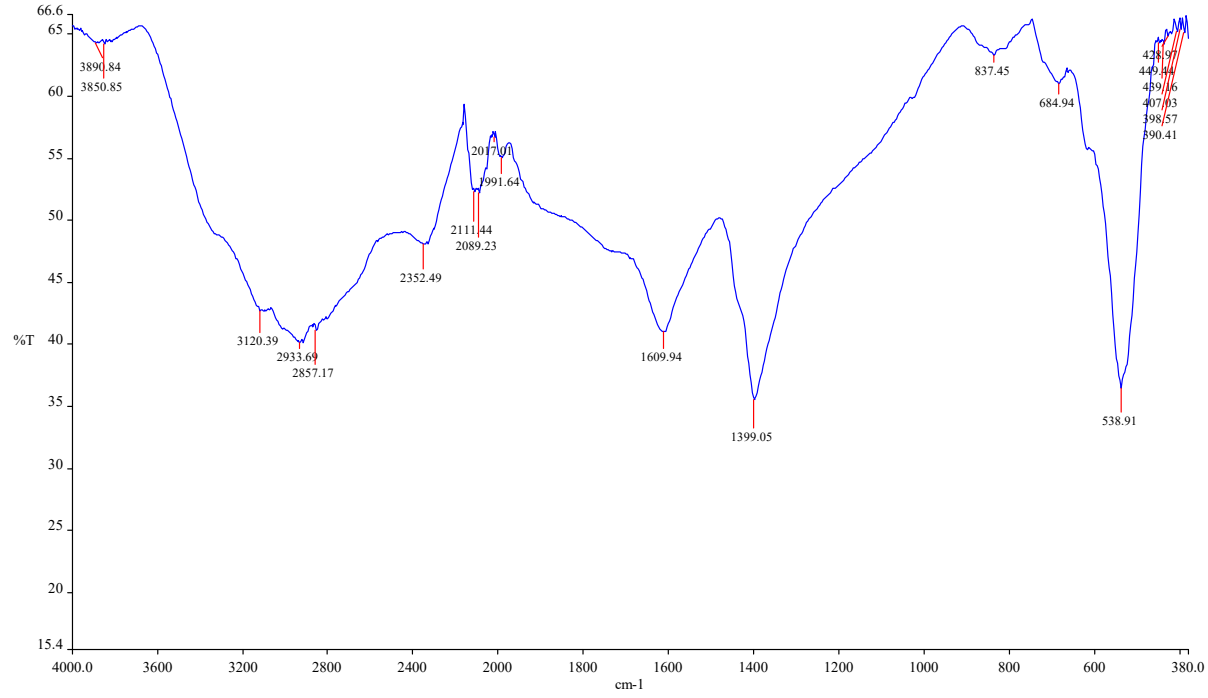

Fig. 8: FTIR spectrum of synthesized magnetite nanoparticles

3.2.3 FTIR spectra of Graphene Oxide nanoparticles

The FTIR spectrum of GO (Fig. 9) shows a broad peak between 3100 –3700 cm^{-1} in the high frequency area corresponding to the stretching and bending vibration of OH groups of water molecules adsorbed on graphene oxide. Therefore, it can be concluded that the sample has strong hydrophilicity. The absorption peaks at 2122 cm^{-1} represent the symmetric and anti-symmetric stretching vibrations of CH_2, while the presence of two absorption peaks observed in the medium frequency area, at 1620 cm^{-1} and 1713 cm^{-1} is attributed to the stretching vibration of C=C and C=O of carboxylic acid and carbonyl groups present at the edges of graphene oxide (Guo *et al.,* 2009). The absorption peak at 1111 cm^{-1} correspond to the stretching vibration C=O of carboxylic acid. The presence of these different types of oxygen functionalities indicates that the graphite was completely oxidized.

3.2.4 FTIR spectra of GO-Fe_3O_4 nanoparticles before and after adsorption

The FTIR spectrum of GO-Fe_3O_4 is shown in Fig. 10. The stretching vibrations of C-O (1111 cm^{-1}) and O-H band (3390 cm^{-1}) for GO appeared at 1101 cm^{-1} and 3323 cm^{-1} respectively for GO-Fe_3O_4.

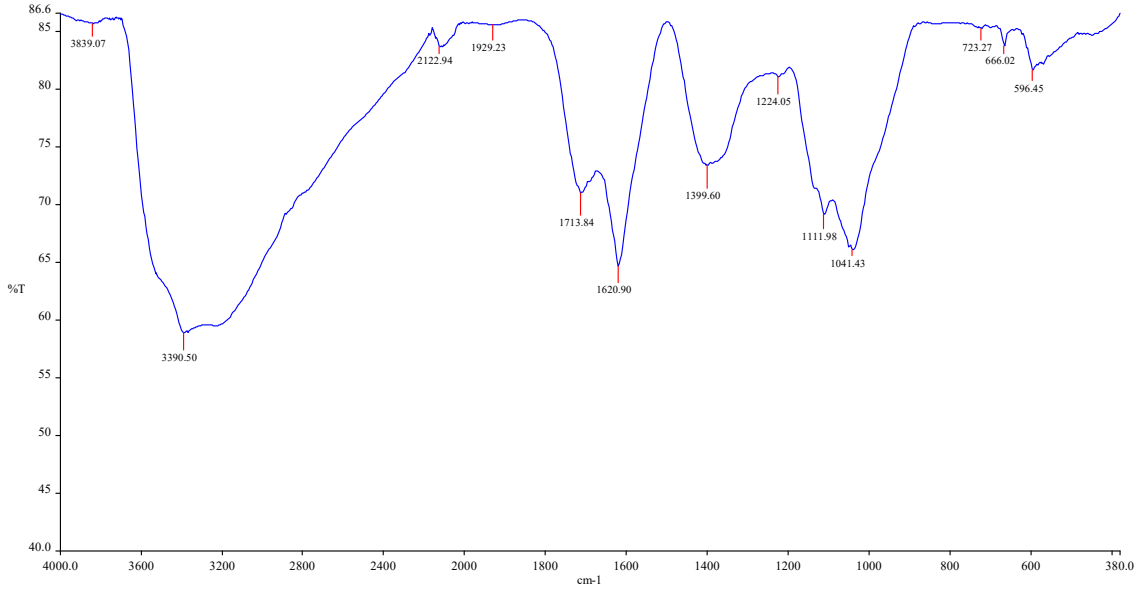

Fig. 9: FTIR spectrum of synthesized GO nanoparticles

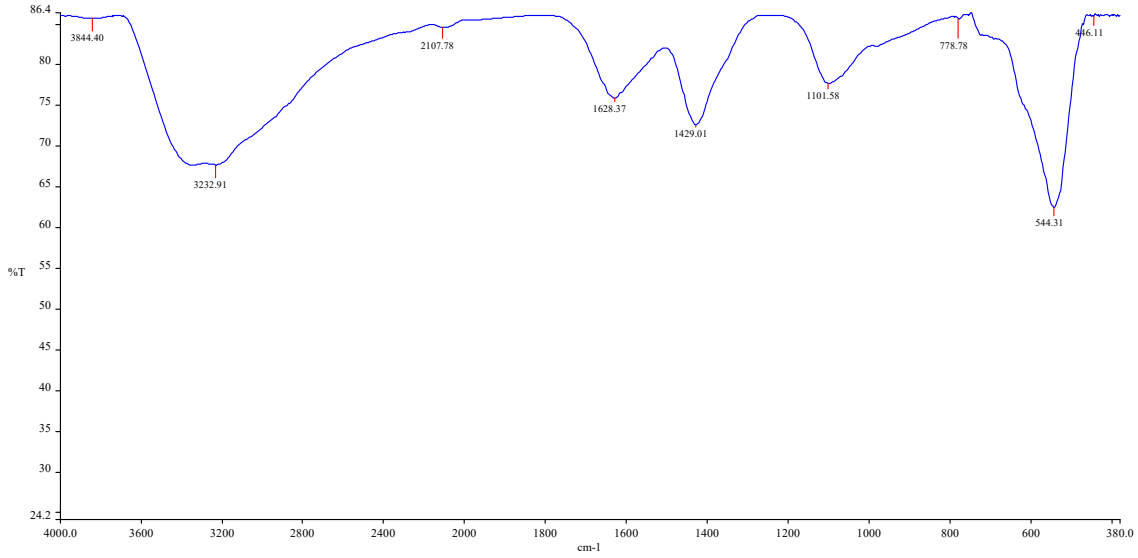

Fig. 10 FTIR spectrum of synthesized GO-Fe_3O_4 nanocomposite

The peak around 1429 cm^{-1} is due to the vibration of O-C=O group. The peak at 1620 cm^{-1} corresponding to stretching frequency of (C=C) of –COOH on GO was observed to have been shifted to 1628 cm^{-1} due to the formation of –COO after coating with Fe_3O_4. The characteristic peak of Fe_3O_4 could also be observed at 544 cm^{-1}, which demonstrated that the Fe_3O_4 nanoparticles were combined with GO with no obvious change.

3.2.5 FTIR spectra of chitosan and chitosan-Fe_3O_4 nanoparticles

The FTIR spectra of chitosan and Fe_3O_4–chitosan nanoparticles were also analysed and the spectra obtained are shown in Figs. 11(a-b). The broad and steep band observed at 3445 cm^{-1} is native for hydroxyl stretching vibration in chitosan. Also, the broad peak observed around 3395 cm^{-1} for Fe_3O_4–chitosan spectrum also corresponds to the hydroxyl stretching vibrations. In the IR spectrum of chitosan (Fig. 11a), the characteristic absorption bands appeared at 1558 and 1641 cm^{-1} which were assigned to N–H bending vibration. Others were at 1415 cm^{-1} (corresponds to C-H bending vibrations) 1381 cm^{-1} (related to –C–O stretching of the primary alcoholic group in chitosan). The adsorption bands at 2920 and 2853 cm^{-1} are attributed to the asymmetric and symmetric CH_2 stretch vibrations of chitosan, respectively. The spectrum of Fe_3O_4–chitosan nanocomposite (Fig. 11b), showed characteristic Fe-O adsorption band which shifted from 538 to 564 cm^{-1}, confirming the presence of magnetite nanoparticles in the samples.

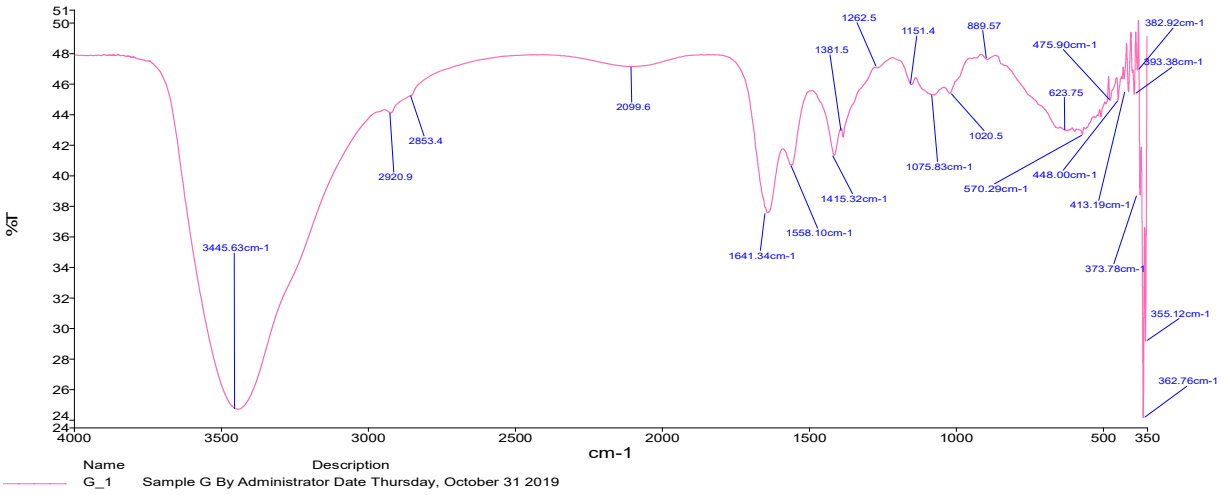

Fig. 11a FTIR spectrum of chitosan

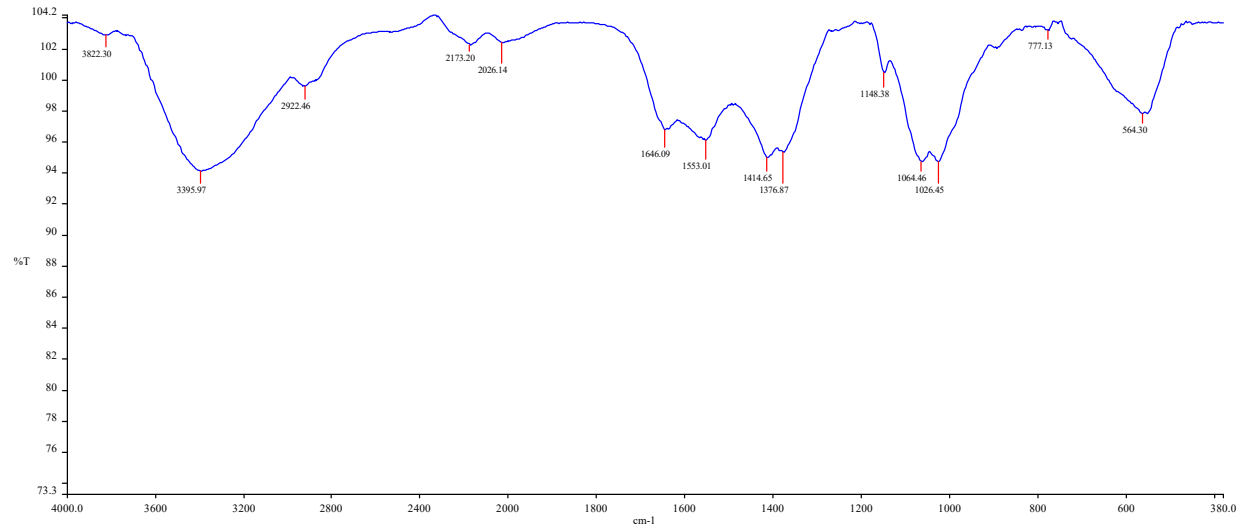

Fig. 11b FTIR spectrum of synthesized chitosan-magnetite nanoparticles

The characteristic bands of saturated C–H absorption shifted to 2922 cm^{-1} with the disappearance of the peak at 2853 cm^{-1}. The low intensity of this peak may be due to the shielding effect of the chitosan coating (Thinh *et al*., 2012). The peaks at 1558 and 1641 cm^{-1} peaks due to N–H bending vibration shifted to 1553 cm^{-1}, and 1646 cm^{-1} respectively. These bands indicated possible binding of the magnetite nanoparticles to NH_2 group of chitosan. Besides, electrostatic interaction between surface negative charged Fe_3O_4 and positively protonated chitosan can also contribute to this IR change (Hasan *et al.,* 2006). This confirmed successful coating of the magnetic nanoparticle with the chitosan polymer and no chemical bonding between chitosan and Fe_3O_4 was formed.

3.3 XRD ANALYSIS

3.3.1 XRD patterns of ZnO

Fig. 12 shows the XRD patterns of ZnO, peaks corresponding to the crystal planes of (100), (002) and (101) of ZnO along with less noise which suggest that the synthesized sample belong to the hexagonal crystal lattice of the ZnO (JCPDS: 65-3411) (Mirzaei *et al.* 2018, Elumalai and Velmurugan, 2015).

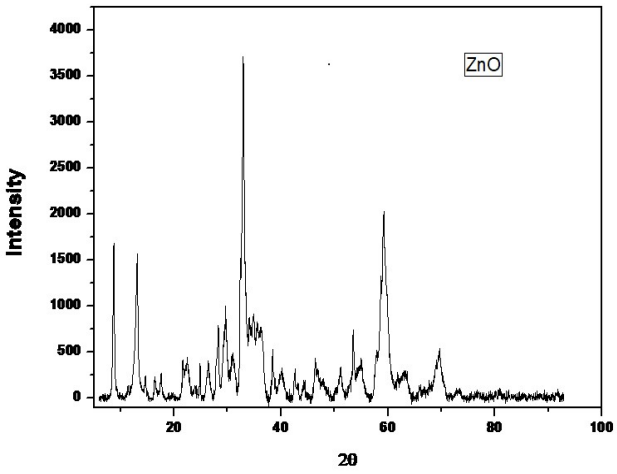

Fig. 12: XRD pattern of synthesized ZnO nanoparticles

The spectra also suggest that the presence of other phases is negligible. The peaks observed were sharp, which indicates that only ZnO compound is present with minimum noise distortion or impurities. From the XRD data, it was found that the peaks are broad; suggesting that the crystallites have sizes in the nanometer range. The calculated average crystallite size of the ZnO nanoparticles was about 9 nm.

3.3.2 XRD patterns of magnetite

The XRD patterns of magnetite (Fig. 13), shows that the magnetite sample had peaks at 2θ of 30.36, 35.74, 43.52, 53.95, 57.34 and 63.0° representing the corresponding indices of (220), (311), (400), (422), (511), and (440) respectively (Cornwell and Schwertmann, 2003; Xu *et al.,* 2010). These were compatible with the standard data for Fe_3O_4 peaks (JCPDS: 19-0629). Calculations performed according to Scherrer equation showed that the average crystallite size of synthesized magnetite was 6.4 nm.

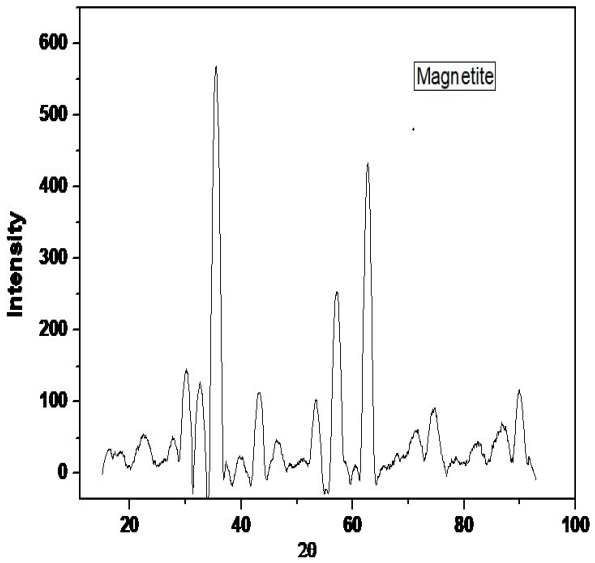

Fig. 13 XRD pattern of synthesized magnetite nanoparticles

3.3.3 XRD patterns of GO nanosheets

Fig. 14 shows the X-ray diffraction pattern (XRD) of GO nanosheets synthesized by modified Hummer's method. The prominent peak (002) which appears at 2θ = 12.13° has an interlayer spacing distance of 0.729 nm, calculated from Braggs equation. Hence, it signifies the complete synthesis of GO. This increase in inter-layer spacing distance indicates that there is intercalation of oxygen functional groups and water molecules into the carbon (graphite) layer (Shahriary, 2014). Another very weak diffraction peak at (2θ = 24.35°) shows peak either for reduced Graphene Oxide (rGO) or Graphite, having an inter-layer spacing distance of 0.365 nm. The observed significant decrease in spacing can be attributed to the elimination of functional group and vanishing of inter-layer attractive interaction of GO. There is also a weak diffraction peak at about 44.5°, which may

be due to incomplete oxidation of graphite (Sharma *et al.,* 2017). The stacking height (crystallite size) and the number of layers was found to be 7.9 nm and 12 respectively as calculated from Scherrer equation and d-spacing for the synthesized graphene oxide.

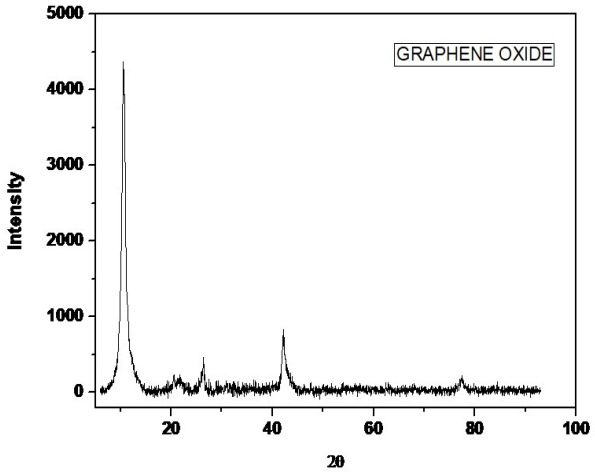

Fig. 14 XRD pattern of synthesized graphene oxide

3.3.4 XRD patterns of GO-magnetite nanocomposites

XRD pattern for GO-magnetite nanocomposites showed characteristic peaks located at 2θ = 30.1, 35.5, 43.2, 53.5, 57.1 and 62.7°, corresponded to the (200), (311), (400), (422), (511) and (440) planes of magnetite of Fe_3O_4 phase (Fig. 15). These peaks are consistent with the database in JCPDS file (PDF No. 65-3107). These peaks were seen placed on an amorphous peak; the amorphous peak can be attributed to GO. The XRD pattern for GO-Fe_3O_4 shows no diffraction peaks for the layered GO, this indicates the absence of layer stacking regularity after Fe_3O_4 deposition. The broad diffraction peaks are indications of the nanoparticles with very small sizes. The crystal size was calculated to be 7.1 nm, for the nanocomposite. The change in size, could be explained by the presence of GO, since GO will prevent the growth and agglomeration of Fe_3O_4 nanoparticles (Perez, 2016).

3.3.5 XRD patterns of Magnetite and chitosan-magnetite

Fig. 16 shows the XRD patterns for the Fe_3O_4 nanoparticles coated with chitosan (chitosan-magnetite nanocomposite). Characteristic peaks for Fe_3O_4 marked by their indices (2 2 0), (3 1 1), (4 0 0), (4 2 2), (5 1 1) and (4 4 0) were observed for the sample. These peaks are consistent with the database in JCPDS file (PDF No. 65-3107) and reveal that the resultant nanoparticles were pure Fe_3O_4.

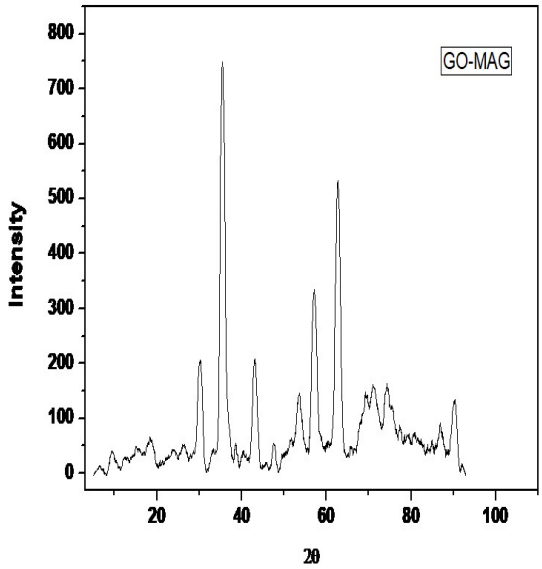

Fig. 15: XRD pattern of synthesized graphene oxide - magnetite nanocomposites

Weak diffraction lines of composite patterns indicated that Fe_3O_4 particles have been coated by amorphous chitosan. Also, the coating process did not result in the phase change of Fe_3O_4. The broad nature of the diffraction bands in the pattern below is an indication of small particle sizes, the crystallite sizes were quantitatively evaluated from the XRD data and found to be 11.2 nm.

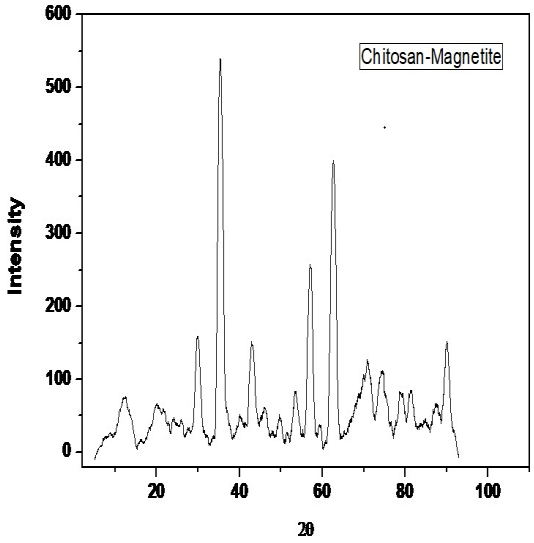

Fig. 16 XRD pattern of synthesized chitosan-nagnetite nanocomposites

4.0 Conclusions

The wet chemical technique is a promising method for the constant and scalable synthesis of various nanomaterials. In this work the syntheses of metal oxides and carbon-based nanoparticles and nanocomposites using the wet chemical methods were successfully established and characterized as shown in the FESEM, EDX, FTIR and XRD analyses. Particles of uniformed shapes and relatively varied sizes were obtained. ZnO nanoparticles were observed to be flake-like and porous with a crystallite size of 9 nm. The magnetite nanoparticles formed were spherical and clumped having a crystallite size of about 6.4 nm. The GO had a loose sponge-like layered structure, its stacking height (crystallite size) and number of layers were found to be 7.9 nm and 12 respectively. The graphene oxide sheets were well distributed between the agglomerated Fe_3O_4 nanoparticles, the XRD result showed that the presence of GO the growth of Fe_3O_4 nanoparticles, thereby reducing the crystallite size to 7.1 nm. Evenly distributed tiny spherical beads of chitosan-magnetite nanocomposite with crystallite size of 11.2 nm were obtained and finally no phase change was observed in the magnetite when combined with both chitosan and GO.

6.0 References

Ayrat,, M. D. & James, M. T. (2014). Mechanism of graphene oxide formation. *ACS Nano,* 8 , 3, pp.3060-3068.

Chang, Y. C., Chang, S. W. & Chen, D. H. (2006). Magnetic chitosan nanoparticles: Studies on chitosan binding and adsorption of Co(II) ions. *Reactive & Functional Polymer* 66, pp. 335-341.

Cornwell, R. M. & Schwertmann, U. (2003). T*he iron oxides. structure, properties, reactions, occurrences and uses*. Sed. Edition, Wiley-VCHGmbh&Co. Weinheim.

Dhillon, G. S., Kaur, S. & Brar, S. K. (2014). Facile fabrication and characterization of chitosan-based zinc oxide nanoparticles and evaluation of their antimicrobial and antibiofilm activity. *International Nano Letters,* 4, 107. doi.org/10.1007/s40089-014-0107-6

Edelstein, A. S. & Cammaratra, R. C. (1998). *Nanomaterials: synthesis, properties and applications*. CRC Press, Taylor and Francis group, London.

Eldin, W., Chuan, L. & Ruili, F. (2012). Agglomeration of magnetic nanoparticles *Journal of Chemical Physics,* 136: 124109, doi. doi:10.1063/1.3697865

Elumalai, K. & Velmurugan, S. (2015). Green synthesis, characterization and antimicrobial activities of zinc oxide nanoparticles from the leaf extract of *Azadirachta indica (L.). Applied Surface Science.* 345, pp. 329-336.

Guo, H.-L., Wang, X.-F., Qian, Q.-Y., Wang, F.-B. & Xia, X.-H. (2009). A Green Approach to the Synthesis of Graphene Nanosheets. *ACS Nano,* 3, 9, pp. 2653–2659

Hasan, S., Krishnaiah, A., Ghosh, T. K., Viswanath, D. S., Boddu, V. M. & Smith, E. D. (2006). Adsorption of Divalent Cadmium (Cd(II)) from Aqueous Solutions onto Chitosan-Coated Perlite Beads. *Industrial & Engineering Chemistry Research,* 45, 14, pp. 5066-5077.

Hong, R. Y., Li, J. H. Chen, L. L., Liu, D. Q., Li, H. Z., Zheng, Y. & Ding, J. (2009). Synthesis, surface modification and photocatalytic property of ZnO nanoparticles. *Powder Technology* 189, pp. 426-432.

Iravani, S. (2011). Green synthesis of metal nanoparticles using plants. *Green Chemistry,* 13,10, pp. 2638.

Keiner, S. (2008). Room at the Bottom?" Potential State and Local Strategies for Managing the Risks and Benefits of Nanotechnology." Washington D.C, Woodrow Wilson International Center for Scholars -*Project on emerging nanotechnologies.*

Kumar, S., Bhushan, P. & Bhattacharya, S. (2017). F*abrication of nanostructures with bottom-up approach and their utility in diagnostics, therapeutics, and others. environmental*, *Chemical and Medical Sensors, pp.* 167-198.

Liu, D., Li, C., Zhou, F., Zhang, T., Zhang, H., Li, X., Duan, G., Cai, W. & Li, Y (2015). Rapid synthesis of monodisperse Au nanospheres through a laser irradiation -induced shape conversion, self-assembly and their electromagnetic coupling SERS enhancement**.** *Scientific Report,* 5, pp. 1-9.

Lubick, N., and Betts, K., (2008). Silver socks have cloudy lining, Court bans widely used flame retardant. *Environmental Science and Technology*, 42, 11, pp. 3910-3910.

Ma, M., Zhang, Y., Yu, W., Shen, H., Zhang, H. & Ning, G. (2003). Preparation and Characterization of Magnetite Nanoparticles Coated by Amino Silane. *Colloids and Surfaces A: Physicochemical and Engineering Aspects*. 212, pp.219-226.

Mirzaei, H. R., Pourghadamyari, H., Rahmati, M., Mohammadi, A., Nahand, J. S., Rezaei, A. & Hadjati, J. (2018). Gene-knocked out chimeric antigen receptor (CAR) T cells: Tuning up for the next generation cancer immunotherapy. *Cancer Letters*, 423, pp. 95-104..

Odiongenyi, A. O. & Afangide, U. N. (2019). Adsorption and thermodynamic studies on the removal of congo red dye from aqueous solution by alumina and nano-alumina. *Communication in Physical Sciences,* 4,1, pp. 1-7.

Odiongenyi, A. O. (2019). Removal of ethyl violet dye from aqueous solution by graphite dust and nano graphene oxide synthesized from graphite dust. *Communication in Physical Sciences*, 4, 2, pp. 103-109.

Pottathara, Y. B., Grohens, Y., Kokol, V., Kalarikkal, N., & Thomas, S. (2019). Synthesis and processing of emerging two-dimensional nanomaterials. *Nanomaterials Synthesis, 1–25.*

Ramos, A. P., Cruz, M., Tovani, C. B. & Ciancaglini, P. (2017). Biomedical applications of nanotechnology. *Biophysical reviews*, 9, 2, pp. 79-89.

Ren, Y., Abbood, H. A., He, F., Peng, H. & Huang, K. (2013). Magnetic EDTA-modified chitosan/SiO2/Fe3O4 adsorbent: Preparation, characterization, and application in heavy metal adsorption. *Chemical Engineering Journal,* 226, pp.300-311.

Rosi, N. L and Mirkin, C. A. (2005). Nanostructures in biodiagnostics. *Chem Rev.* 105: 1547–1562.

Sangeetha, G., Rajeshwari, S. & Venckatesh, R (2011). Green synthesis of zinc oxide nanoparticles by *Aloe barbadensis miller* leaf extract: structure and optical properties. *Materilas Research Bulletin*, 46, 12, pp. 2560–2566.

Savasari, M., Emadi, M., Bahmanyar, M. A. & Biparva, P. (2015). Optimization of Cd (II) removal from aqueous solution by ascorbic acid-stabilized zero valent iron nanoparticles using response surface methodology. *Journal of Industrial and Engineering Chemistry,* 21, pp. 1403-1409.

Shahriary, L. & Athawale, A. A. (2014). Graphene Oxide Synthesized by Using Modified Hummers Approach. *International Journal of Renewable Energy and Environmental Engineering,* 2, pp. 58-63.

Sharma, R., Chadha, N. & Saini, P. (2017). Determination of defect density, crystallite size and number of graphene layers in graphene analogues using X-ray diffraction and Raman spectroscopy. *Indian Journal of Pure and Applied Physics,* 55, 9, pp. 625-629.

Thinh, N. N. Hanh, P. T., Ha, T. T., Anh, N. , Hoang, T. V ., Hoang, V. D. , Dang, H ., Khoi, N. V. & Lam, T. D (2012). Magnetic chitosan nanoparticles for removal of Cr(VI) from aqueous solution. *Materials Science and Engineering*, C33, pp. 1214–1218.

Vaishnavi S., Kiruba D., Ruckmani, K. & Sivakumar, M. (2015). Fabrication of chitosan–magnetite nanocomposite strip for chromium removal, *Applied Nano Science*, 6, pp. 77–285.

Wang, Y. & Xia, Y. (2004). Bottom-Up and Top-Down Approaches to the Synthesis of Monodispersed Spherical Colloids of Low Melting-Point Metals. *Nano Letters*, 4, 10, pp. 2047-2050.

Wang, Y., Zhang, C., Bi, S. & Luo, G. (2010), Preparation of ZnO nanoparticles using the direct precipitation method in a membrane dispersion micro-structured reactor. *Powder Technology,* 202, pp. 130-136.

Xu, L. Feng, J. Li, J. Liu, X. & Jiang, S. (2012). "Graphene oxide bonded fused-silica fiber for solid-phase microextraction-gas chromatography of polycyclic aromatic hydrocarbons in water," Journal of Separation Science, 35, 1, pp. 93-100.

Zaka, A. K., Abd. Majid, W. H., Darroudi, M. & Yousefi, R. (2011). Synthesis and characterization of ZnO nanoparticles prepared in gelatin media. *Materials Letters*, 65, pp. 65:70-73.

Zhou, H., Yi, R., Li, J., Su, Y., and Liu, X. (2010). Microwave-assisted synthesis and characterization of hexagonal Fe_3O_4 nanoplates. *Solid State Sciences,* 12, 1, pp. 99-104.